The Astrophysical Journal, 863:36 (4pp), 2018 August 10 https://doi.org/10.3847/1538-4357/aacf07

Fourier Transform Spectroscopy of the $C^3\Delta$–$X^3\Delta$ Transition of TiO in Support of Exoplanet Spectroscopy

James N. Hodges and Peter F. Bernath
Department of Chemistry and Biochemistry, Old Dominion University, Norfolk, VA 23529, USA
Received 2018 May 31; accepted 2018 June 22; published 2018 August 8

Abstract

Recent limitations in the TiO line list used in cross-correlation detection schemes have made the detection and quantification of TiO in exoplanetary atmospheres challenging. The quality of the line list appears to degrade at wavelengths shorter than 630 nm. The $C^3\Delta$–$X^3\Delta$ electronic transition has strong rovibronic bands near 500 nm. In an effort to improve the line list, a spectrum of TiO in a furnace at 1950 K is analyzed, and the assigned lines of the $C^3\Delta$–$X^3\Delta$ transition are fit with the $\hat{N}^2$ Hamiltonian in the molecular spectrum fitting software, PGOPHER. Several newly determined molecular constants are reported and the average error in fitting the line positions is 0.017 cm^{-1} or ~1 ppm relative error. The new line positions are expected to resolve any problems with cross-correlation templates near 500 nm.

Key words: astrochemistry – methods: laboratory: molecular – molecular data

Supporting material: machine-readable table

1. Introduction

TiO is an astrophysically relevant near-infrared and visible absorber (McKemmish et al. 2017). Spectral features of TiO are typically observed in M-type dwarfs (Allard et al. 2000; Lodders 2002), and are proposed to be present in the atmospheres of hot Jupiter exoplanets (Désert et al. 2008). Ordinarily, metal containing molecules are not expected to be present in exoplanet atmospheres. However, for atmospheres at temperatures greater than 1800 K that are strongly irradiated by the star they orbit, thermal inversion layers can exist. The existence of these layers are often caused by strongly absorbing species like TiO present in the atmosphere (Seager & Sasselov 1998; Hubeny et al. 2003; Fortney et al. 2008).

Efforts to detect TiO in the atmospheres of exoplanets have produced mixed results. Huitson et al. (2013) failed to detect TiO in WASP-19b. In contrast, Evans et al. (2016) found evidence for TiO in the ultra-hot atmosphere of WASP-121b. More recently, Evans et al. (2017) confirmed the existence of a stratosphere in the atmosphere of WASP-121b but did not require the inclusion of TiO lines in their atmospheric model. Nevertheless, they claim TiO may still be present and responsible for the thermal inversion layer. A survey of 30 exoplanets by Tsiaras et al. (2018) also supported the presence of TiO in WASP-121b, but the detection is not conclusive. Similarly, Stevenson et al. (2014) made a possible detection of TiO in the atmosphere of WASP-12b. However, this is not in agreement with the optical survey conducted by Sing et al. (2013).

Hoeijmakers et al. (2015) conducted a search for TiO in the atmosphere of HD 209458b. Désert et al. (2008) proposed TiO to be responsible for the broadband absorption in the optical region and low albedo of HD 209458b. Hoeijmakers et al. (2015) used cross-correlation of HD 209458b spectra with a template based on the line list from Freedman et al. (2008) based on the earlier work of Schwenke (1998). Hoeijmakers et al. (2015) were unable to detect TiO in the spectra of HD 209458b and checked their template against the TiO rich spectrum of Barnard's Star. They found reasonable correlation at longer wavelengths but little or no correlation at wavelengths shorter than 630 nm. The failure at shorter wavelengths suggests that the TiO line list can be improved.

Efforts to use templates that do not utilize shorter wavelengths have been successfully employed to detect TiO in the atmosphere of WASP-33b (Nugroho et al. 2017) at high spectral resolution. Likewise, the detection of TiO by transit spectroscopy was made in the atmosphere of WASP-19b by Sedaghati et al. (2017) using strong bands at wavelengths longer than 600 nm. Tsiaras et al. (2018) used near-infrared spectral features to detect TiO in the atmosphere of WASP-76b by transit spectroscopy with the *Hubble Space Telescope*. The necessity to exclude the shorter wavelength portion of the spectrum and the conflicting evidence regarding detection of TiO in the atmospheres of WASP-12b and HD 209458b indicate that the TiO molecular line list should be revisited and updated. More confidence in the line list will both enable and better constrain detections, which would improve the modeling of hot Jupiter exoplanets.

Recent efforts to address the deficiency in the line list have been made by Bittner & Bernath (2018), who reanalyzed the singlet transitions, and by the Measured Active Rotational-Vibrational Energy Level (MARVEL) analysis of TiO by McKemmish et al. (2017). In short, MARVEL is an algorithm that inputs the available spectroscopic data, transition assignments, and measurement uncertainties to determine the energy levels and their associated uncertainties. The TiO MARVEL analysis covers the 2–22,160 cm^{-1} region and uses 24 literature sources containing 49,679 transitions. Of those transitions 48,590 were validated and used to determine the energy levels.

The careful analysis by Hoeijmakers et al. (2015) of their TiO template demonstrated a failure in the shorter wavelength region where the $C^3\Delta$–$X^3\Delta$ band system (hereafter *C*–*X*) exists. A good summary of the previous *C*–*X* work is presented by Namiki et al. (2003) wherein they fit the *C*–*X* bands including a spin–orbit perturbation of $C^3\Delta$ state by the $c^1\Phi$ state. However, no new spectroscopic data was presented by Namiki et al. (2003).

Here, we analyze a high-quality Fourier transform emission spectrum of the *C*–*X* transition. We were able to determine more complete molecular parameters for the $C^3\Delta$ $v = 0$, 1, and 2 vibrational levels. In order to properly constrain the perturbation of the $C^3\Delta$ $v = 2$ level, we also fit the $c^1\Phi$–$a^1\Delta$

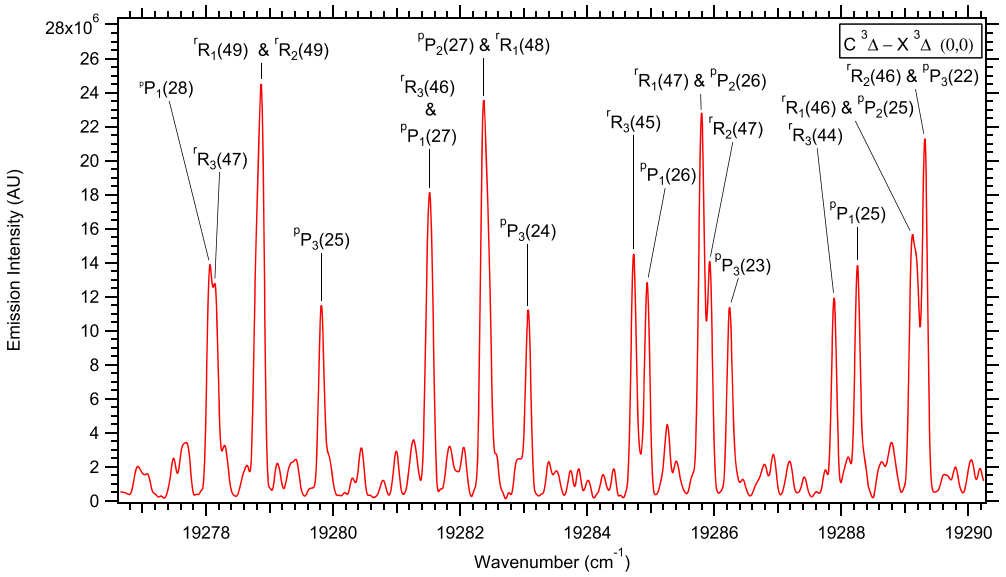

Figure 1. Rotationally resolved, representative portion of the $C^3\Delta$–$X^3\Delta$ (0, 0) band. The labels correspond to the branch label of the emission line.

Table 1
Spectroscopic Constants for the $C^3\Delta$ Excited State

Constants	$v = 0$ (cm^{-1})	$v = 1$ (cm^{-1})	$v = 2$ (cm^{-1})
T_v	19339.77422(46)	20168.49733(57)	20989.062(15)
B_v	0.48829816(61)	0.48515507(45)	0.4818960(54)
$D_v/10^{-7}$	6.6938(21)	6.75211(83)	6.653(15)
$H_v/10^{-12}$	−0.052(24)	−0.0195(41)	−2.83(24)
$L_v/10^{-18}$	2.58(91)	⋯	279(19)
$M_v/10^{-20}$	⋯	⋯	−1.049(54)
A_v	48.64939(22)	48.56925(30)	48.731(11)
$A_{Dv}/10^{-4}$	2.3828(11)	2.4115(14)	2.130(28)
$A_{Hv}/10^{-8}$	−0.1303(46)	−0.1345(57)	2.37(18)
$A_{Lv}/10^{-12}$	⋯	⋯	−2.318(78)
λ_v	−1.15576(48)	−1.40924(61)	−1.164(11)
$\lambda_{Dv}/10^{-5}$	0.969(58)	3.683(40)	4.15(29)
$\lambda_{Hv}/10^{-9}$	−0.52(14)	−1.781(40)	−4.15(50)
$\lambda_{Lv}/10^{-13}$	−0.64(14)	⋯	7.27(53)
$\alpha_{red}(C \sim c)$	⋯	⋯	40.67(17)

Note. Values in parenthesis represent 1σ standard deviation.

$(v' = 0, v'' = 0)$ band present in our spectrum. We expect these new molecular constants and our observed line list to improve the spectroscopy of TiO in exoplanetary atmospheres.

2. Experimental

The experimental spectrum of TiO was recorded in 1985 at the McMath–Pierce Solar Telescope using the 1 m Fourier transform spectrometer, operated by the National Solar Observatory at Kitt Peak. The spectrum (850116R0.002) was recorded by S. Davis, G. Stark, J. Wagner, and R. Hubbard from emission of a carbon furnace at 1950 K at a pressure of about 50 Torr. The total acquisition time was about 1.5 hrs, with a total of 13 scans. The spectral resolution was 0.044 cm^{-1}. A UV beam splitter was used in conjunction with a CG495 colored glass filter. Blue-enhanced photodiodes were used to detect the light.

We used a zero fill factor of four and calibrated the spectrum with the strongest $A^3\Phi$–$X^3\Delta$ TiO transitions as reported by Ram et al. (1999), which results in a calibration accuracy of 0.004 cm^{-1}. The quality of the calibration is sufficient so that the predominant uncertainty in our measurements is due to the precision, which we estimate (in the standard way) to be one-half the FWHM divided by the signal-to-noise ratio (S/N).

Table 2
Spectroscopic Constants for the $v = 0$ Levels of the $c^1\Phi$ and $a^1\Delta$ Excited States

Constants	$c^1\Phi$ (cm^{-1})	$a^1\Delta$ (cm^{-1})
T_0	21181.529(47)	3346.3358(23)
B_0	0.523253(23)	0.536169(11)
$D_0/10^{-7}$	9.94(23)	4.99(14)
$H_0/10^{-10}$	1.87(12)	−0.466(58)
$L_0/10^{-14}$	−5.65(22)	⋯
$M_0/10^{-18}$	4.53(19)	⋯

Note. Values in parenthesis represent 1σ standard deviations.

3. Results and Discussion

The calibrated TiO spectrum was assigned and fit using the standard $\hat{N}^2$ Hamiltonian in the program PGOPHER (Western 2017). The ground state $X^3\Delta$ molecular parameters were held fixed to the values determined by Ram et al. (1999). Then initial guesses were made for the line parameters of the $C^3\Delta$ vibrational levels based on Namiki et al. (2003). We began by assigning and fitting the intense emission from the $C^3\Delta$–$X^3\Delta$ (0, 0), (0, 1), and (1, 0) bands. Based on the average S/N and linewidth of these bands, we assigned a fit uncertainty of 0.0085 cm^{-1}, 0.009 cm^{-1}, and 0.0085 cm^{-1}, respectively. The resulting molecular parameters are presented in Table 1. Due to the high temperature of the furnace spectrum, many rotational lines were observed, which allowed us to unambiguously assign 1330 transitions in the (0, 0) band, 1334 in the (1, 0), and 1203 in the (0, 1) band.

A small sample of the spectrum is presented in Figure 1. The S/N can be deceptive in the figure because of the large number of lines. The spectral line density is high due to emission from other TiO isotopologues, overlapped vibrational bands, and the

Table 3
Portion of the Line List Used in the Fit

η'	v'	J'	N'	F_n' Parity	η''	v''	J''	N''	F_n'' Parity	Branch Label	λ (Å)	Wavenumber (cm^{-1})	Obs.−Calc. (cm^{-1})
C	$v = 0$	103	102	F1e	X	$v = 0$	104	103	F1e	pP1e(104)	5334.0579	18742.2395	−0.0075
C	$v = 0$	103	102	F1f	X	$v = 0$	104	103	F1f	pP1f(104)	5334.0579	18742.2395	−0.0075
C	$v = 2$	64	63	F1e	X	$v = 2$	65	64	F1e	pP1e(65)	5333.9395	18742.6554	0.0297

Note. The table includes the upper and lower electronic states, the upper and lower quantum numbers, and each transition's branch label. The transition frequency is reported as the wavelength in standard air and wavenumbers adjacent to the fit residual.

(This table is available in its entirety in machine-readable form.)

high temperature. The small features in Figure 1 are emission lines and not the noise floor. The labeled lines all belong to the (0, 0) band and are labeled according to the spectroscopic convention.

The weaker emission from the $C^3\Delta$–$X^3\Delta$ (1, 1) band was not observed. We attribute this to the significantly smaller Franck–Condon factor, which is about 100 times smaller than for the (0, 0), (1, 0), and (0, 1) bands (Namiki et al. 2003). After successfully determining the molecular constants for the $C^3\Delta$ $v = 0$, 1 levels, we attempted to assign bands involving the $C^3\Delta$ $v = 2$ levels. The (2, 1) and (2, 2) bands are difficult to distinguish because they are overlapped with the (1, 0) and (0, 0) bands and are weaker in intensity. The (2, 0) band was not present in our spectrum. In order to locate lines connecting to $C^3\Delta$ $v = 2$, we used archival data for the (2, 0) band from McKemmish et al. (2017) and references therein.

In order to fit the (2, 0) band, a spin–orbit perturbation between the $C^3\Delta_3$ $v = 2$ and $c^1\Phi_3$ $v = 0$ levels needed to be accounted for. Fortunately, PGOPHER is readily able to accommodate user-specified perturbations. The operator added to the Hamiltonian in PGOPHER is of the form $\hat{L} \cdot \hat{S}$, and the end result is the addition of the following matrix elements to the Hamiltonian:

$$\langle C, v = 2, J, \Lambda = -2, \Omega = -3|\hat{L} \cdot \hat{S}|c, v = 0, J, \Lambda = -3, \Omega = -3\rangle = \frac{\alpha_{\rm red}(C \sim c)}{\sqrt{3}} \quad (1)$$

$$\langle C, v = 2, J, \Lambda = 2, \Omega = 3|\hat{L} \cdot \hat{S}|c, v = 0, J, \Lambda = 3, \Omega = 3\rangle = -\frac{\alpha_{\rm red}(C \sim c)}{\sqrt{3}}. \quad (2)$$

A fit uncertainty of $0.035\,cm^{-1}$ was chosen to be representative of the (2, 0) band data set based on the average reported uncertainties in the archival data. Again, initial guesses were taken from Namiki et al. (2003). Care must be taken when using the initial guess of the perturbation. The perturbation strength reported by PGOPHER is in terms of a reduced matrix element, i.e., with the Wigner 3j symbol factored out. It is more typically reported with the 3j symbol included as is the case in Namiki et al. (2003). The $\alpha_{\rm red}(C \sim c)$ parameter is the reduced form of the $\alpha(C \sim c)$ parameter of Namiki et al. (2003) and can be directly compared by dividing by $\sqrt{3}$.

In order to constrain the value of the perturbation matrix element, the $c^1\Phi$–$a^1\Delta$ (0, 0) band was fit, which is also present in our spectrum. We assigned 120 lines in our spectrum to this band. This band could not be fit alone because the transition network must be relative to the ground state. This means the band origin for the $c^1\Phi$ $v = 0$ level cannot be determined on the same energy scale as the $C^3\Delta$ $v = 2$ level without the inclusion of additional transitions. In order to tie the band origins of the $c^1\Phi$ $v = 0$ level and the $a^1\Delta$ $v = 0$ levels to the ground state, the $C^3\Delta$–$a^1\Delta$ (2, 0) triplet-to-singlet band as recorded by Kaledin et al. (1995) was included in the fit. The $c^1\Phi$–$a^1\Delta$ (0, 0) was assigned a $0.01\,cm^{-1}$ uncertainty according to a its average S/N in our spectrum. The $C^3\Delta$–$a^1\Delta$ (2, 0) was assigned a $0.01\,cm^{-1}$ uncertainty based on the resolution of the experiment (Kaledin et al. 1995). Inclusion of these singlet states allowed us to properly assess the magnitude of the matrix element. The determined parameters for the singlets are listed in Table 2.

After the C–X (2, 0) band was included in the fit, we were able to confidently pick the lines of the (2, 1) and (2, 2) bands out of the congested spectrum. We assigned 1076 transitions from the (2, 1) band and 820 from the (2, 2) band. We assigned a $0.011\,cm^{-1}$ uncertainty to the (2, 1) band and a $0.02\,cm^{-1}$ uncertainty to the (2, 2) band based on the lower S/N of the two bands. After all the bands were included, the final molecular parameters are listed in Table 1. A summary of the all the transitions and line positions can be found in Table 3. The line positions are reported in wavenumbers and wavelength in standard air calculated using the refractive index formula from Birch & Downs (1994), and the updated equation originally from Edlén (1966).

The quality of the fit is good as the weighted residuals are evenly distributed within $\sim 3\sigma$. The average unweighted error for the total fit is $0.017\,cm^{-1}$, about 1 ppm relative error, and the chosen errors assigned to each band in the fit (described above) appear to be accurate assessments of the uncertainties. The results from the fit represent an improvement over the previous molecular constants as reported by Namiki et al. (2003). This is in part because of the high temperature of the furnace, which ensures that high J transitions are detected. Additionally, the accuracy of the calibration and the high S/N ensure data used in the fit have an excellent frequency determination.

For the $C^3\Delta$ state, we were able to determine 12 new molecular constants, all with a higher order of centrifugal distortion than the previously determined constants. By necessity, we were also able to determine three additional molecular constants in the $c^1\Phi$ and $a^1\Delta$ states. The addition of these higher order distortion constants will measurably improve the quality of the calculated positions of previously unobserved lines, which will be useful for simulating spectra in environments that are hotter than that of the furnace in this experiment.

The spectrum that we analyzed is particularly relevant to hot Jupiter atmospheres, and the line list that we provide will be useful in a follow-up MARVEL analysis similar to that performed by McKemmish et al. (2017) or by directly using

our line positions (observed or calculated) as an input to an atmospheric model. Ultimately, these measurements will improve the templates at wavelengths shorter than 630 nm, where Hoeijmakers et al. (2015) identified the limitations of the previous line list.

4. Conclusions

Previous work by Hoeijmakers et al. (2015) identified limitations in the line list of TiO. In order to partly address this limitation, we have assigned the $C^3\Delta$–$X^3\Delta$ band system in a spectrum of TiO measured at the National Solar Observatory. The assigned lines were fit to the standard $\hat{N}^2$ Hamiltonian in PGOPHER, which resulted in the determination of a number of additional molecular constants for the $C^3\Delta$ $v = 0$, 1, and 2 levels. The average accuracy of the fit is 0.017 cm^{-1} (1 ppm relative error), though individual bands have lower uncertainties. The reported line positions of TiO are expected to be useful in improving the existing atmospheric templates.

The National Solar Observatory (NSO) is operated by the Association of Universities for Research in Astronomy, Inc. (AURA), under cooperative agreement with the National Science Foundation. The spectrum was recorded by S. Davis, G. Stark, J. Wagner, and R. Hubbard and was obtained from the NSO data archives. Financial support was provided by the NASA exoplanet program (grant NNX16AB51G).

Software: PGOPHER (Western 2017).

ORCID iDs

Peter F. Bernath https://orcid.org/0000-0002-1255-396X

References

Allard, F., Hauschildt, P. H., & Schwenke, D. 2000, ApJ, 540, 1005
Birch, K. P., & Downs, M. J. 1994, Metro, 31, 315
Bittner, D. M., & Bernath, P. F. 2018, ApJS, 236, 46
Désert, J.-M., Vidal-Madjar, A., Lecavelier des Etangs, A., et al. 2008, A&A, 492, 585
Edlén, B. 1966, Metro, 2, 71
Evans, T. M., Sing, D. K., Kataria, T., et al. 2017, Natur, 548, 58
Evans, T. M., Sing, D. K., Wakeford, H. R., et al. 2016, ApJL, 822, 1
Fortney, J. J., Lodders, K., Marley, M. S., & Freedman, R. S. 2008, ApJ, 678, 1419
Freedman, R. S., Marley, M. S., & Lodders, K. 2008, ApJS, 174, 504
Hoeijmakers, H. J., de Kok, R. J., Snellen, I. A. G., et al. 2015, A&A, 575, A20
Hubeny, I., Burrows, A., & Sudarsky, D. 2003, ApJ, 594, 1011
Huitson, C. M., Sing, D. K., Pont, F., et al. 2013, MNRAS, 434, 3252
Kaledin, L., McCord, J., & Heaven, M. 1995, JMoSp, 173, 499
Lodders, K. 2002, ApJ, 577, 974
McKemmish, L. K., Masseron, T., Sheppard, S., et al. 2017, ApJS, 228, 15
Namiki, K.-I. C., Ito, H., & Davis, S. P. 2003, JMoSp, 217, 173
Nugroho, S. K., Kawahara, H., Masuda, K., et al. 2017, AJ, 154, 221
Ram, R. S., Bernath, P. F., Dulick, M., & Wallace, L. 1999, ApJS, 122, 331
Schwenke, D. W. 1998, FaDi, 109, 321
Seager, S., & Sasselov, D. D. 1998, ApJL, 502, L157
Sedaghati, E., Boffin, H. M. J., MacDonald, R. J., et al. 2017, Natur, 549, 238
Sing, D. K., Lecavelier des Etangs, A., Fortney, J. J., et al. 2013, MNRAS, 436, 2956
Stevenson, K. B., Bean, J. L., Seifahrt, A., et al. 2014, AJ, 147, 161
Tsiaras, A., Waldmann, I. P., Zingales, T., et al. 2018, AJ, 155, 156
Western, C. M. 2017, JQSRT, 186, 221